Proceedings of the 2022 Design of Medical Devices Conference
DMD2022
April 11-14, 2022, Minneapolis, MN, USA

DMD2022-1008

ESTIMATION OF TISSUE MOVEMENT IN NEEDLE INSERTION TASKS USING AN ACTIVE NEEDLE

Blayton Padasdao
University of Hawaii at Manoa
Honolulu, HI

Zolboo Batsaikhan
University of Hawaii at Manoa
Honolulu, HI

Dailen Brown
The Pennsylvania State University
University Park, PA

Jason Moore
The Pennsylvania State University
University Park, PA

Bardia Konh[1]
University of Hawaii at Manoa
Honolulu, HI

ABSTRACT

Needle insertion has been used as a minimally invasive technique in many diagnostic or therapeutic procedures such as prostate biopsy or brachytherapy. While the success of these procedures relies on accurate positioning of the needle tip at target positions, the intraoperative movement of the tissue (and consequently the target) has caused physicians some difficulties in acquiring the target. This paper presents a method to estimate tissue movement during a needle insertion task within tissue. The movement of the tissue is valuable information for guidance, navigation, and control of the needle inside tissue towards the target. A needle insertion task was performed using an active needle bending. Ultrasound images were captured at four needle insertion stages of initial needle insertion, bending, unbending, and needle retraction. Ultrasound images were then analyzed to estimate the tissue movement at each stage. The study showed that needle retraction, insertion, bending, and unbending stages correspond to largest to lowest tissue movement, respectively.

Keywords: Tissue deformation, target movement, acquiring target, needle insertion

1. INTRODUCTION

Needle insertion is a common less-invasive approach in procedures such as ablation, brachytherapy, and biopsy. Medical imaging is critical for tracking the needle while operating within the patient's body. Ultrasound (US) imaging has widely been used to track the needle trajectory inside tissue toward the desired target [1,2]. For example, in prostate brachytherapy, physicians utilize US images to detect the needle tip at the target (i.e., malignant tissue) and implant radioactive seeds to irradiate cancerous cells locally. Medical imaging allows for real-time and intraoperative needle tip trajectory tracking, which can be utilized to calculate the deviation from a preplanned trajectory. The deviation can be used as feedback in needle navigation closed-loop control systems for accurate targeting [3]. Reed et al. [4] developed a system that guides the needle and prevents it to move out of the plane by integrating a 2D planner, visual feedback, and a linearized controller. A 3D US tracking was employed in another study to put an active cannula at a desired target [5]. Pepley [6] developed and tested simulation of US tissue-needle deformation using passive needles for traditional manikin and cadaver training. Maier-Hein et al. [7] have developed the target position estimation accuracy for minimally invasive interventions utilizing liver tissue motion simulator. Other works [8,9] developed a force-based analytical model for needle-tissue interaction using bevel-tipped needles.

It still remains challenging to accurately guide the needle inside the tissue due to (i) anatomical false features in the US images that may be mistaken with the needle, (ii) movement of the target, (iii) poor quality of the US images, and (iv) tissue movement. Tissue deformation and movement of the target are among the system uncertainties that are especially difficult to predict. The needle motion and the consequent tissue movement introduce uncertainties in the intraoperative position of target and path planning. Prediction of the intraoperative movement of target during a needle insertion task could enhance closed-loop control systems and consequently improve targeting accuracy.

This work aims to provide a method for estimating the tissue movement in a needle insertion task using an active needle.

[1] Contact Author: konh@hawaii.edu

2. MATERIALS AND METHODS

The following sections explain experimental methods to estimate tissue movement while an active needle is inserted and actuated inside a phantom tissue. Section 2.1 discusses the active needle and manipulation system for the needle insertion task, and Section 2.2 details the methodology for analyzing the US images (captured in real time) to estimate tissue movement.

2.1 Experimental Setup with Ultrasound Tracking

A tendon-driven active needle (Figure 1) [10–12] was used in this work for needle insertion tests in phantom tissues. The needle tube was a superelastic nitinol tube (Goodfellow Cambridge Ltd., Cambridge, UK) with an outer and inner diameter of 1.8mm and 1.5mm, respectively with a wall thickness of 0.15mm. Six cuts were made on the needle tube (average width of 0.3mm and depth of 1.4mm) to create a flexible section. Other research groups (Okamura [13], Webster [14], Desai [15], Esashi [16], and Armand [17]) have previously employed cut-out patterns (notches) of various designs and sizes on a superelastic nitinol tube for improved flexibility of the needle. The cuts were made in the lab using normal machining tools such as a Dremel and ultra-thin cut-off discs with a thickness of 0.2mm (Gesswein & Co., Inc., Bridgeport, Connecticut). A custom-made fixture was used to hold the needle in place for machining (creating the cuts) and to move the needle precisely at predetermined intervals between the cuts. The phantom tissue was a polyvinylchloride (PVC) gel (M-F Manufacturing Co., Ft. Worth, TX), with 3:1 ratio of plastic (PVC suspension) to softener with an indentation elastic modulus of about 25.6±0.6 kPa.

FIGURE 1: (A) UNBENT TENDON-DRIVEN ACTIVE NEEDLE USED IN THIS WORK TO DETERMINE TISSUE MOVEMENT DURING NEEDLE ACTUATION. (B) BENT CONFIGURATION OF THE ACTIVE NEEDLE OBSERVED IN AIR.

A shape memory alloy wire (0.13mm diameter) was used as a tendon to bend the needle within the tissue. Two holes with a diameter of about 0.8mm were made close to the distal end of the needle to host the tendon. The tendon was looped in and out of these holes, applying pulling forces to the needle, and thereby bending in the direction of the cuts.

The active needle was visualized inside the tissue using an US machine (Chison, Eco 5) with a Chison L7 Linear Array US transducer. Sagittal US images were captured along the needle shaft to estimate tissue deformation (explained in next section).

To control actuation of the needle, a pulling mechanism combination shown in Figure 2 was developed. The combination consists of a 0.5W Maxon DC motor (RE 8 Ø8 mm, Precious Metal Brushes) with an 8mm diameter lead screw drive (GP 8 S Ø8mm, Metric spindle, M3 x 0.5), and an encoder (MR, Type S, 100CPT). The Maxon motor was connected to a computer using a EPOS4 digital positioning controller via USB and programmed using Maxon Group's software, EPOS Studio. The software communicates with Maxon Group's EPOS4 positioning controller to give the user control on the position, velocity, and acceleration profiles.

Two holders were designed, and 3D printed to hold the motor and the lead screw (shown in Figure 2). Holder 1, housing a nut on the lead screw, was mounted on a 50mm long linear rail guide (MGN9H) to translate rotational movement of the motor shaft to linear movement. Holder 2 was stationary, keeping the position of the motor. The holders are designed to ensure that all the movement occurs on the same plane. The free end of the tendon was fixed on Holder 1. The tendon is threaded through the midpoint of the holder to ensure collinear movement.

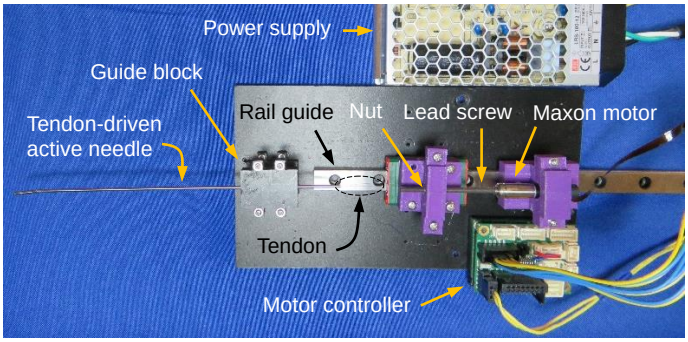

FIGURE 2: ACTUATION AND CONTROL SYSTEM TO PULL THE TENDON AND BEND THE NEEDLE ASSEMBLED ON A LINEAR STAGE.

The Maxon motor, gear box, and lead screw were mounted on a linear stage for needle insertion tests in a phantom tissue. The Maxon motor pulls the tendon axially to bend the needle. The motor is fixed to a linear motion guide rail with the lead screw nut being held in place on a movable platform along the rail. The needle is considered at its maximum bending position when the tendon is pulled 3.5mm in the axial direction, causing the cuts in the needle to touch each other.

2.2 Tissue Movement Analysis

The recorded ultrasound videos were processed in MathWorks (Natick, MA) MATLAB using the Farnebäck estimation method. The Farnebäck algorithm produces an image pyramid, with each level having a lower resolution than the previous one. When a pyramid level larger than one is selected, the algorithm follows the points at different resolution levels, beginning with the lowest. By increasing the number of pyramid layers, the algorithm can manage larger point displacements between frames. The algorithm illustrates 3 pyramid levels and a neighborhood size of 9 pixels. Quiver

[1] Contact Author: konh@hawaii.edu

plots of the optical flow were generated for every 10th frame of the video during the sections of the video in which the needle was inserted, bent, unbent, and retracted. The direction and magnitude of each resulting vector field were plotted by pixel to generate useful visualizations of each stage of the needle insertion.

3. RESULTS AND DISCUSSION

Figures 3-6 show different stages in a needle insertion process: (i) initial needle insertion, (ii) needle bending, (iii) needle unbending, and (iv) needle retraction. The stages were chosen to closely mimic clinical needle insertion tasks. From there, the greatest tissue environment disturbance could be determined, however many factors such as needle tip design, needle material, etc. could influence this motion. The needle was inserted into the phantom tissue to a depth of 45mm (entering from the left side of the US image).

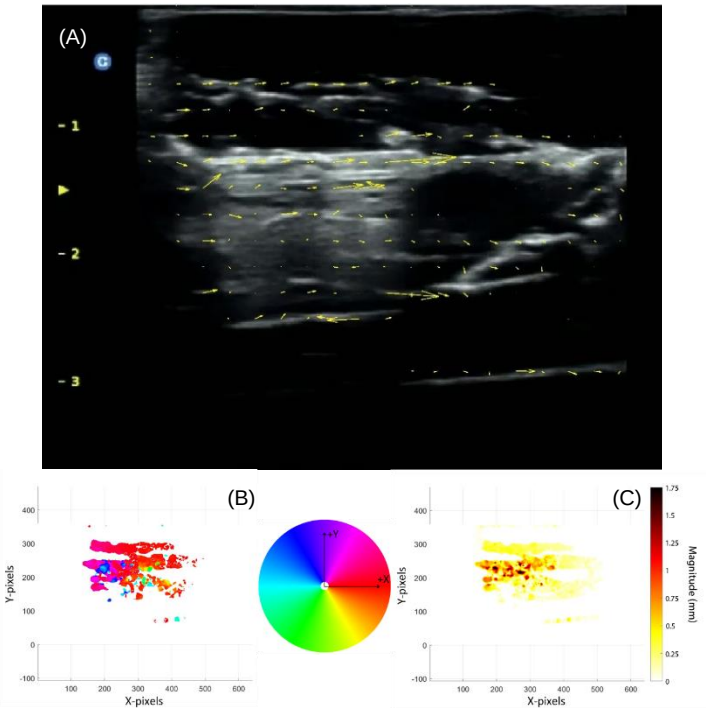

FIGURE 3: (A) QUIVER PLOT OF 2D SAGITTAL US IMAGE WITH VECTOR FIELD OVERLAY FOR NEEDLE INSERTION, (B) DIRECTIONAL SURFACE PLOT TO SHOW PIXEL MOVEMENT, AND (C) MAGNITUDE SURFACE PLOT TO SHOW THE AMOUNT OF PIXEL MOVEMENT.

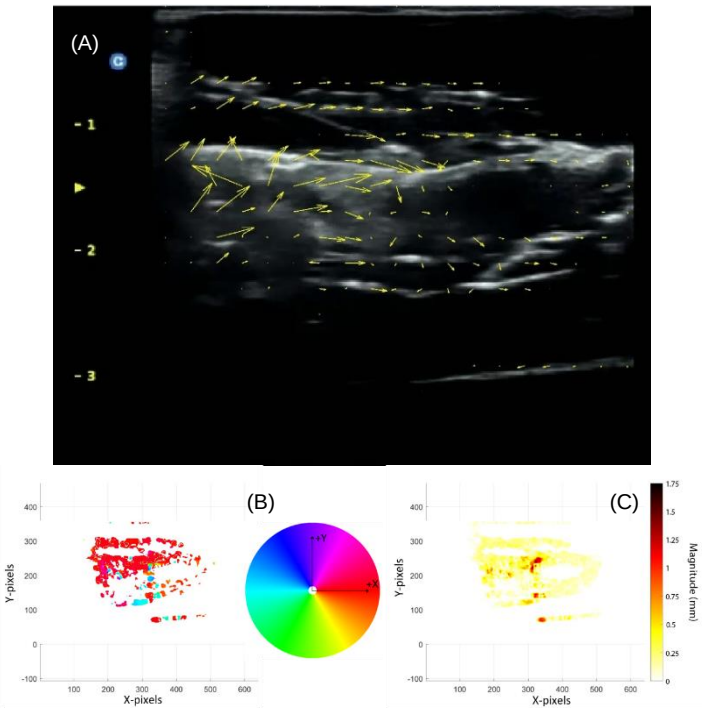

FIGURE 4: (A) QUIVER PLOT OF 2D SAGITTAL US IMAGE WITH VECTOR FIELD OVERLAY FOR NEEDLE BENDING, (B) DIRECTIONAL SURFACE PLOT TO SHOW PIXEL MOVEMENT, AND (C) MAGNITUDE SURFACE PLOT TO SHOW THE AMOUNT OF PIXEL MOVEMENT.

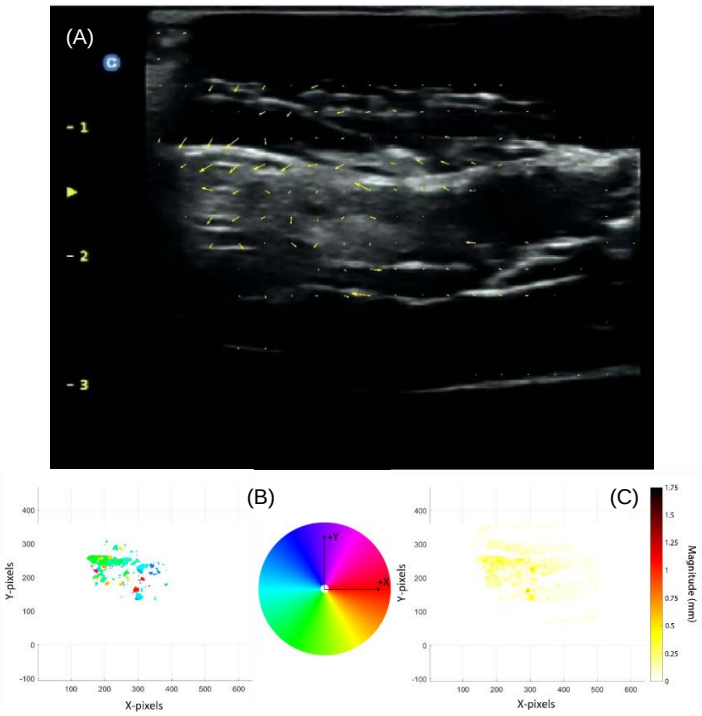

FIGURE 5: (A) QUIVER PLOT OF 2D SAGITTAL US IMAGE WITH VECTOR FIELD OVERLAY FOR NEEDLE UNBENDING, (B) DIRECTIONAL SURFACE PLOT TO SHOW PIXEL MOVEMENT, AND (C) MAGNITUDE SURFACE PLOT TO SHOW THE AMOUNT OF PIXEL MOVEMENT.

[1] Contact Author: konh@hawaii.edu

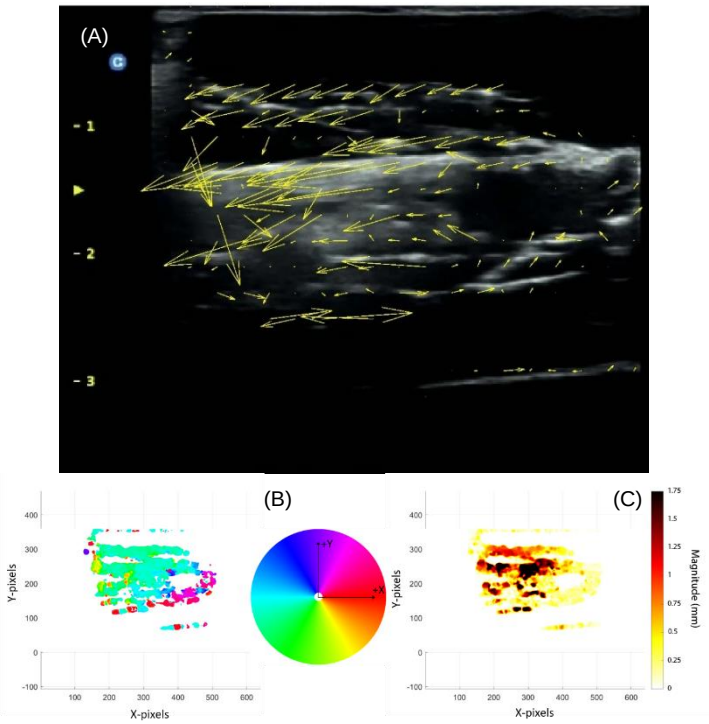

FIGURE 6: (A) QUIVER PLOT OF 2D SAGITTAL US IMAGE WITH VECTOR FIELD OVERLAY FOR NEEDLE RETRACTION, (B) DIRECTIONAL SURFACE PLOT TO SHOW PIXEL MOVEMENT, AND (C) MAGNITUDE SURFACE PLOT TO SHOW THE AMOUNT OF PIXEL MOVEMENT.

Once the needle reaches this depth, the tendon is pulled to realize a 40-degree bend within the phantom tissue, causing the needle tip to bend downward in the US images. The tendon is then relaxed to unbend the needle. Finally, the needle is retracted from the phantom tissue. The subfigures labeled as "A" in the following figures depict the quiver plot of the vector field overlayed on the US screen illustrating the tissue movement from frame to frame. The subfigures labeled as "B" depict the directional surface plot of the direction that each pixel moves. Each color signifies a direction that corresponds to the color wheels in Figures 3-6 with the color white signifying no movement. Finally, the subfigures labeled as "C" depict the magnitude surface plot of the amount that each pixel moves with the darker areas signifying greater displacement. Needle retraction, bending, insertion, and unbending stages resulted in largest to lowest tissue movement, respectively.

4. CONCLUSION

A method was presented in this work to estimate the tissue movement at four stages of a needle insertion task: insertion, bending, unbending, and retraction. Estimation and prediction of the tissue movement caused by the steerable active needle is valuable information in needle steering towards the target in closed-loop feedback control system. Largest to lowest tissue movement was estimated at needle retraction and needle insertion, needle bending, and needle unbending, respectively, with future work being planned for testing the force applied to the tissue environment at different phases to determine the magnitude of tissue damage.

ACKNOWLEDGEMENTS

This work was funded in part by Hawaii Community Foundation, Grant ID # 20ADVC-102159, in part by University of Hawaii (UH) Cancer Center's SITS (Strategic Investment in Translational Science) program, and in part by The National Institute of Biomedical Imaging and Bioengineering of the National Institutes of Health under Award Number 1K25EB030562-01A1. The content is solely the responsibility of the authors and does not necessarily represent the official views of the National Institutes of Health.

REFERENCES

[1] Konh, B., Padasdao, B., Batsaikhan, Z., and Ko, S. Y., 2021, "Integrating Robot-assisted Ultrasound Tracking and 3D Needle Shape Prediction for Real-time Tracking of the Needle Tip in Needle Steering Procedures," Int. J. Med. Robot. Comput. Assist. Surg., **17**(4), p. 2272.

[2] Konh, B., Batsaikhan, Z., and Padasdao, B., 2021, "3D Shape Estimation of an Active Needle inside Tissue Using 2D Ultrasound Images," *Design of Medical Devices Conference*, pp. 1–4.

[3] Cowan, N. J., Goldberg, K., Chirikjian, G. S., Fichtinger, G., Alterovitz, R., Reed, K. B., Kallem, V., Park, W., Misra, S., and Okamura, A. M., 2011, "Robotic Needle Steering: Design, Modeling, Planning, and Image Guidance," *Surgical Robotics*, Springer, Boston, MA, pp. 557–582.

[4] Reed, K. B., Kallem, V., Alterovitzt, R., Goldberg, K., Okamura, A. M., and Cowan, N. J., 2008, "Integrated Planning and Image-Guided Control for Planar Needle Steering," *Proceedings of the 2nd Biennial IEEE/RAS-EMBS International Conference on Biomedical Robotics and Biomechatronics, BioRob 2008*, pp. 819–824.

[5] Swaney, P. J., Burgner, J., Pheiffer, T. S., Rucker, D. C., Gilbert, H. B., Ondrake, J. E., Simpson, A. L., Burdette, E. C., Miga, M. I., and Webster III, R. J., 2012, "Tracked 3D Ultrasound Targeting with an Active Cannula," *Medical Imaging 2012: Image-Guided Procedures, Robotic Interventions, and Modeling*, p. 83160R.

[6] Pepley, D. F., Adhikary, S. D., Miller, S. R., and Moore, J. Z., 2019, "Simulating Ultrasound Tissue Deformation Using Inverse Mapping," J. Comput. Nonlinear Dyn., **14**(10), pp. 1–8.

[7] Maier-Hein, L., Müller, S. A., Pianka, F., Seitel, A., Müller-Stich, B. P., Gutt, C. N., Rietdorf, U., Richter, G., Meinzer, H.-P., Schmied, B. M., and Wolf, I., 2007, "In-Vitro Evaluation of a Novel Needle-Based Soft Tissue Navigation System with a Respiratory Liver Motion Simulator," *Proceedings of SPIE*, SPIE, pp.

[1] Contact Author: konh@hawaii.edu

650916–6509112.
[8] Misra, S., Reed, K. B., Ramesh, K. T., and Okamura, A. M., 2009, "Observations of Needle-Tissue Interactions," Conf. Proc. (IEEE Eng. Med. Biol. Soc. Conf.), **2009**, pp. 262–265.
[9] Datla, N. V., Konh, B., Honarvar, M., Podder, T. K., Dicker, A. P., Yu, Y., and Hutapea, P., 2014, "A Model to Predict Deflection of Bevel-Tipped Active Needle Advancing in Soft Tissue," Med. Eng. Phys., **36**(3), pp. 285–293.
[10] Padasdao, B., Varnamkhasti, Z. K., and Konh, B., 2020, "3D Steerable Biopsy Needle with a Motorized Manipulation System and Ultrasound Tracking to Navigate inside Tissue," J. Med. Robot. Res., **5**(03n04), p. 2150003.
[11] Konh, B., Padasdao, B., Batsaikhan, Z., and Lederer, J., 2021, "Steering a Tendon-Driven Needle in High-Dose-Rate Prostate Brachytherapy for Patients with Pubic Arch Interference," *International Symposium on Medical Robotics (ISMR)*, pp. 1–7.
[12] Padasdao, B., Batsaikhan, Z., Lafreniere, S., Rabiei, M., and Konh, B., 2022, "Modeling and Operator Control of a Robotic Tool for Bidirectional Manipulation in Targeted Prostate Biopsy," *International Symposium on Medical Robotics (ISMR)*, pp. 1–6.
[13] Gerboni, G., Greer, J. D., Laeseke, P. F., Hwang, G. L., and Okamura, A. M., 2017, "Highly Articulated Robotic Needle Achieves Distributed Ablation of Liver Tissue," IEEE Robot. Autom. Lett., **2**(3), pp. 1367–1374.
[14] York, P. A., Swaney, P. J., Gilbert, H. B., and Webster, R. J., 2015, "A Wrist for Needle-Sized Surgical Robots," *IEEE International Conference on Robotics and Automation*, pp. 1776–1781.
[15] Chitalia, Y., Jeong, S., Yamamoto, K. K., Chern, J. J., and Desai, J. P., 2020, "Modeling and Control of a 2-DoF Meso-Scale Continuum Robotic Tool for Pediatric Neurosurgery," IEEE Trans. Robot., pp. 1–12.
[16] Haga, Y., Muyari, Y., Goto, S., Matsunaga, T., and Esashi, M., 2011, "Development of Minimally Invasive Medical Tools Using Laser Processing on Cylindrical Substrates," Electr. Eng. Japan, **176**(1), pp. 65–74.
[17] Kutzer, M. D. M., Segreti, S. M., Brown, C. Y., Taylor, R. H., Mears, S. C., and Armand, M., 2011, "Design of a New Cable-Driven Manipulator with a Large Open Lumen: Preliminary Applications in the Minimally-Invasive Removal of Osteolysis," Proc. - IEEE Int. Conf. Robot. Autom., pp. 2913–2920.

[1] Contact Author: konh@hawaii.edu